JACS
JOURNAL OF THE AMERICAN CHEMICAL SOCIETY
Article
pubs.acs.org/JACS

Fluorescence Activation Imaging of Cytochrome c Released from Mitochondria Using Aptameric Nanosensor

Ting-Ting Chen,[†] Xue Tian,[†] Chen-Liwei Liu,[†] Jia Ge,[†] Xia Chu,*[,†] and Yingfu Li[‡]

[†]State Key Laboratory of Chemo/Bio-Sensing and Chemometrics, College of Chemistry and Chemical Engineering, Hunan University, Changsha 410082, P. R. China

[‡]Department of Biochemistry and Biomedical Sciences, McMaster University, Hamilton L8S 4K1, Canada

Supporting Information

ABSTRACT: We have developed an aptameric nanosensor for fluorescence activation imaging of cytochrome c (Cyt c). Fluorescence imaging tools that enable visualization of key molecular players in apoptotic signaling are essential for cell biology and clinical theranostics. Cyt c is a major mediator in cell apoptosis. However, fluorescence imaging tools allowing direct visualization of Cyt c translocation in living cells have currently not been realized. We report for the first time the realization of a nanosensor tool that enables direct fluorescence activation imaging of Cyt c released from mitochondria in cell apoptosis. This strategy relies on spatially selective cytosolic delivery of a nanosensor constructed by assembly of a fluorophore-tagged DNA aptamer on PEGylated graphene nanosheets. The cytosolic release of Cyt c is able to dissociate the aptamer from graphene and trigger an activated fluorescence signal. The nanosensor is shown to exhibit high sensitivity and selectivity, rapid response, large signal-to-background ratio for *in vitro*, and intracellular detection of Cyt c. It also enables real-time visualization of the Cyt c release kinetics and direct identification of the regulators for apoptosis. The developed nanosensor may provide a very valuable tool for apoptotic studies and catalyze the fundamental interrogations of Cyt c-mediated biology.

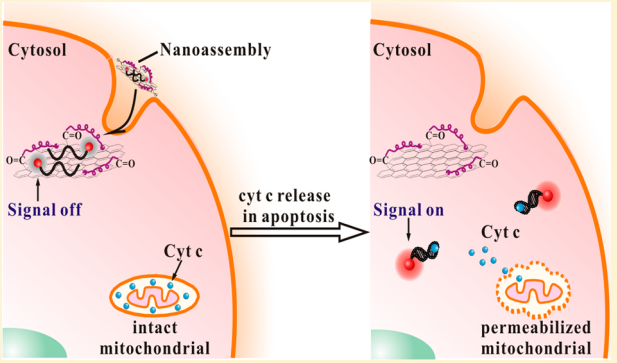

INTRODUCTION

Apoptosis, the process of programmed cell death, is a complex and highly regulated process that has tremendous impact on cell growth and proliferation.[1] Deregulation of apoptosis is closely associated with degenerative disorders (excessive apoptosis), autoimmune disorders and cancers (inadequate apoptosis). Monitoring the progression to apoptosis, elucidating the apoptotic signaling, and developing drugs to modulate apoptotic pathways in living cells are the essential parts of cell biology and clinical theranostics.[2]

Apoptosis occurs through activation of a complex cell suicide process comprising multiple intracellular and extracellular events, such as caspase activation, release of cytochrome c (Cyt c) from mitochondria, externalization of phosphatidylserine on plasma membrane and internucleosomal DNA fragmentation.[3] Unlike phosphatidylserine externalization and DNA fragmentation that are not always associated with apoptosis, caspase activation and Cyt c release are highly specific events in apoptotic signaling. It is recognized that caspases are the key mediators of the induction and execution phase of apoptosis, while Cyt c release is a major caspase activation pathway, often defining the point of no-return in cell apoptosis.[4] Therefore, assays for these specific molecular players in living cells are critical for apoptosis research.

Current techniques have been mainly focused on the imaging of caspase activation in apoptotic cells.[5] Technologies enabling detection of Cyt c translocation in living cells have been rarely explored. Existing technologies for assays of Cyt c release are implemented via fractionation of cell extracts or immunocytochemistry with immobilized cells,[6] which are not suitable for living cell detection. Techniques for live-cell tracking of Cyt c translocation are based on the subcellular localization of Cyt c with a GFP tag or a short tetracysteine label.[7] These techniques, however, require tedious operations to derive cell lines expressing Cyt c fusions and indirect complicated colocalization analysis of Cyt c with mitochondria. Moreover, they are inherently lack of sensitivity for evaluating the translocation of Cyt c in apoptotic cells. Imaging tools allowing direct visualization of Cyt c translocation in living cells have currently not been realized.

Here we report for the first time the realization of a nanosensor tool that enables direct fluorescence activation imaging of Cyt c released from mitochondria in apoptotic cells, as illustrated in Scheme 1. This realization relies on spatially selective internalization of a nanosensor constructed by assembly of a fluorophore-tagged DNA aptamer[8] on PEGylated

Received: November 23, 2014
Published: December 30, 2014

DOI: 10.1021/ja511988w
J. Am. Chem. Soc. 2015, 137, 982−989

Scheme 1. Illustration of Fluorescence Activation Strategy for Cyt c Release Imaging

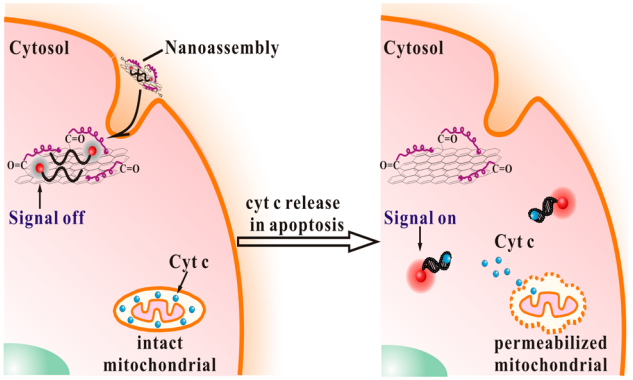

graphene oxide (GO) nanosheets. The nanoassembly displays a very weak fluorescence signal due to highly efficient quenching of the fluorophores on graphene surface.[9] With folate labels introduced at the ends of PEG moieties, the nanoassembly can be efficiently internalized by tumor cells into the cytoplasm while not penetrating into the mitochondria. The spatial isolation of the nanosensor from target Cyt c thus delivers a low fluorescence background. The release of Cyt c from mitochondria into the cytoplasm during cell apoptosis brings Cyt c and the nanoassembly into close interaction, resulting in the formation of aptamer−Cyt c complex with concomitant dissociation of the aptamer from GO surface. An intense fluorescence response is then activated, enabling direct visualization of the Cyt c translocation event. This is also the first time that spatially selective localization of an activatable nanocomplex sensor is developed for a "turn-on" fluorescence imaging mechanism of intracellular translocation events in living cells. This strategy eliminates the need of colocalization analysis for molecular translocation studies. Moreover, the fluorescence activation imaging provides the advantages of being sensitive, real-time and quantitative for detecting the molecular translocation events.

RESULTS AND DISCUSSION

Synthesis and Characterization of Aptamer−GO Nanoassembly. The nanosensor was constructed through noncovalent assembly of the fluorophore-tagged DNA aptamer on GO nanosheets modified with PEGs (MW 1500, length ~15 nm), as shown in Scheme 2. The use of PEG modification was designed to improve the solubility of the nanosensor in cell growth media (Figure S1 in Supporting Information), which was critical for achieving desirable stability of the nanosensor in intracellular imaging applications. For PEGylation of GO, the nanosheets were treated with chloroacetic acid under strongly basic conditions to increase the abundance of carboxylic acid groups on the surface followed by the conjugation with PEG-diamine using the succinimide coupling (EDC-NHS) method.[5b] With the use of this coupling reaction, the residual amino groups of PEG-diamine were further linked to folate, a small-molecule ligand that targets folate receptor (FR) known to have high expression on most of tumor cells.[10] The nanoassembly was obtained by incubation of cyanine 5 (Cy5)-labeled DNA aptamer with the PEGylated GO, allowing the aptamers to be self-assembled on GO surfaces due to $\pi-\pi$ stacking and van der Waals interactions between the DNA and GO.[11]

Scheme 2. Illustration of Synthesis for Aptamer−GO Nanoassembly

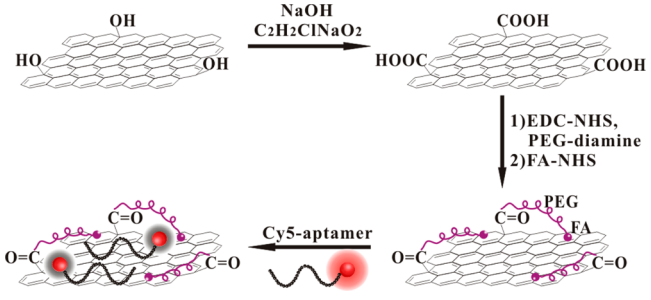

The nanoassembly was characterized by atomic force microscopy (AFM) to profile the morphological changes during the synthesis (Figure 1). Most of GO nanosheets showed a lateral size ranging from 50 to 100 nm (Figure S2 in Supporting Information) with a topological height of ~1 nm, a typical thickness for single-layered GO sheets.[9] After PEGylation, the nanosheets gave a topological height of ~4 nm, evidencing the conjugation of PEG in a lying-down conformation on GO surface. The aptamer−PEGylated GO nanoassembly had an irregular height profile with a bulge of ~10 nm at the central domain, indicators for the assembly of DNA aptamer in a coiled conformation on GO surface. The coverages of PEG and aptamer on GO surface were estimated to be ~8.4×10^{11}/cm^2 and ~3.1×10^{11} /cm^2, respectively. The successful preparation of the nanoassembly was further confirmed using infrared spectroscopy (Figure S3 in Supporting Information).

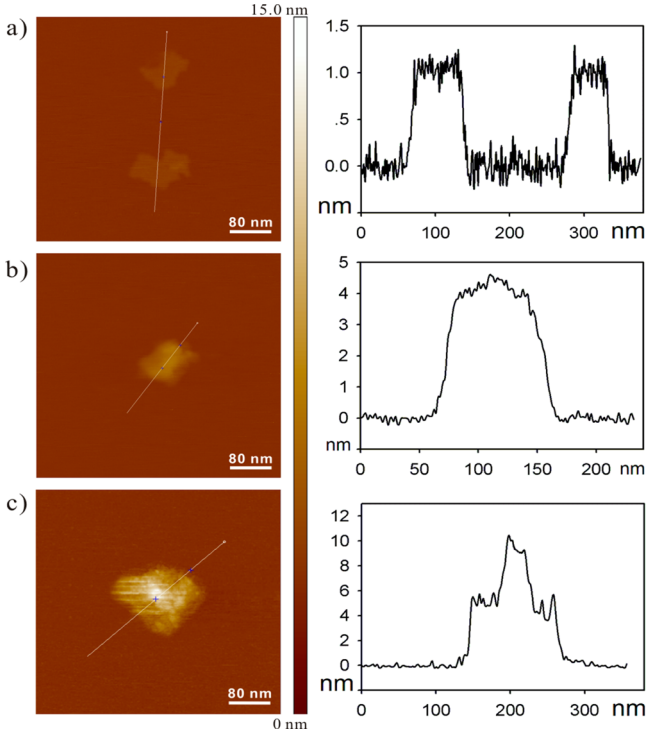

Figure 1. AFM images (left) and height profiles (right): (a) GO, (b) PEGylated GO, (c) aptamer−PEGylated GO nanoassembly.

***In Vitro* Response of Aptamer−GO Nanoassembly.** The as-prepared nanoassembly was found to give very weak fluorescence (0.21% of the intensity for 500 nM aptamer before

DOI: 10.1021/ja511988w
J. Am. Chem. Soc. 2015, 137, 982−989

quenching by 150 μg mL^{-1} GO), indicating very high fluorescence quenching efficiency for Cy5 by GO. By contrast, incubation of the nanoassembly with 10 μM Cyt c resulted in a ~236-fold enhancement of the fluorescence signal, indicating a high signal-to-background response of the nanosensor to target Cyt c (Figure 2a). Fluorescence anisotropy analysis demonstrated that this activated fluorescence was ascribed to the formation of aptamer−Cyt c complex that induces the dissociation of the aptamer from GO surface (Figure S4 in Supporting Information). Moreover, there was no appreciable fluorescence activation when the nanoassembly was incubated with the RPMI 1640 cell growth medium or the plasma extract of nonapoptotic HeLa cells. These observations revealed that the components of the cell growth medium and the cell plasma did not induce dissociation of the DNA aptamer from PEGylated GO surface and thus had no interference with the detection of Cyt c in living cells. Note that Cyt c has an immature form, apocytochrome c, existing in the cytosol and the mature heme-containing Cyt c is present only in the mitochrondria where the heme group is added with an induced conformational change of the protein.[1] No interference from the plasma extract actually suggested that the DNA aptamer had very high specificity in discriminating apocytochrome c from the mature heme-containing Cyt c. Thus, this finding implied the ability of the nanosensor for selective detection of Cyt c released from mitochrondria. A control experiment using another nanoassembly obtained by incubating nonaptamer DNA with PEGylated GO did not give appreciable fluorescence enhancement on incubation with 10 μM Cyt c. This result verified that the fluorescence activation response was specific to the interaction between Cyt c and its aptamer, validating the selectivity of the nanosensor. Further inspection of the fluorescence responses to other components (100 μM) possibly coexisting with Cyt c such as cysteine (Cys), isoascorbic acid (AA), adenosine triphosphate (ATP), insulin, platelet-derived growth factor B-chain (PDGF), vascular endothelial growth factor (VEGF), ferritin, immunoglobulin G (IgG), and human serum albumin (HSA), revealed that these species did not cause remarkable fluorescence recovery (Figure 2b). These data further verified the high selectivity of the nanosensor for Cyt c assay.

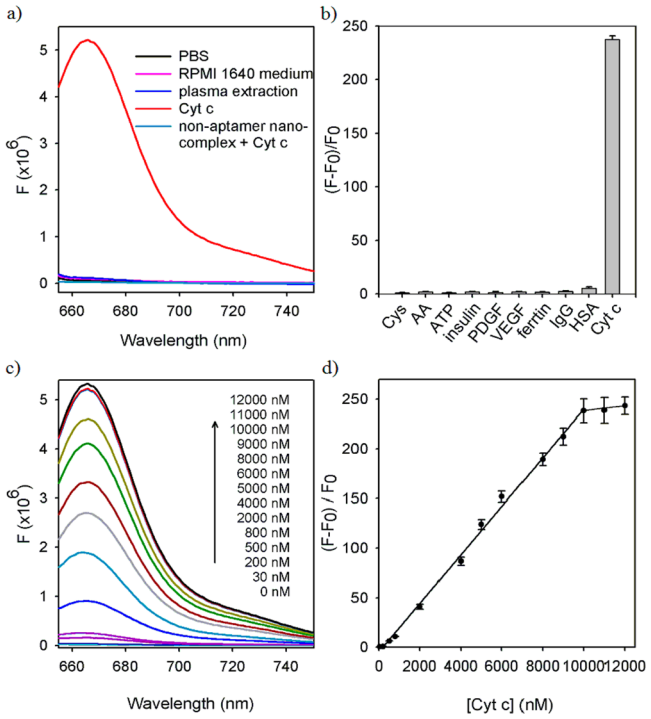

Figure 2. (a) Typical fluorescence spectral responses of nanosensor. Cyt c concentration is 10 μM. (b) Fluorescence peak intensity responses of nanosensor. Cyt c concentration is 10 μM, and concentrations for other species are 100 μM. (c) Fluorescence spectral responses to Cyt c of varying concentrations. (d) Correlation curve of normalized fluorescence peak intensities at 664 nm versus Cyt c concentrations.

Moreover, the nanosensor was found to give fluorescence signals linearly correlated to the concentrations of Cyt c (Figure 2c,d). The linear response range was from 30 nM to 10 μM with a detection limit of 10 nM, covering the literature values (1−10 μM) for cytosolic Cyt c in apoptotic cells.[12] Further improvement of the detection sensitivity could be achieved by using a lower working concentration of the nanoassembly (Figure S5 in Supporting Information). This signified the advantage of adjustable detection ranges of this nanosensor via the use of different nanoassembly concentrations. Taken together, these results revealed that the developed nanosensor could provide a highly sensitive and selective platform with adjustable detection ranges for quantifying Cyt c in apoptosis studies.

Interestingly, we observed PEGylation of GO not only offered better solubility to the nanoassembly in cell growth media, but improved the detection sensitivity (10-fold lower detection limit) and the response kinetics (2.3-fold faster kinetic rate constant) (Figures S6 and S7 in Supporting Information). Presumably, PEGylated GO had less hydrophobic sites where proteins could be nonspecifically adsorbed. The adsorption of target Cyt c restricted its interaction with the aptamer and thus decreased the detection sensitivity and the response kinetics. The higher sensitivity and more rapid response implied the ability of this nanosensor for real-time imaging of the early stage Cyt c translocation event in apoptotic cells. Moreover, we found that the fluorescence responses of the nanosensor to Cyt c of varying concentrations remained unchanged even in the matrix of the plasma extract of nonapoptotic HeLa cells (Figure S8 in Supporting Information). Such transferability of the calibration model from an *in vitro* matrix to an intracellular surrounding indicated the potential of the nanosensor for quantitative imaging of Cyt c in apoptotic cells.

Toxicity of the nanoassembly to living cells was then investigated using HeLa cell line with positive FR expression (FR+). After incubating cells with the nanoassembly of varying concentrations, we observed only marginal toxicity for the nanoassemby at a concentration up to 500 μg mL^{-1} with the cell viability decreased by ~7% after 8 h incubation (Figure S9 in Supporting Information). This data demonstrated the high biocompatibility of the nanoassembly. Moreover, fluorescence imaging of the cells using a commercial intracellular caspase-3 probe revealed that there was no caspase-3 activation even when the cells were incubated for 8 h with the nanoassemby of 500 μg mL^{-1} (Figure S10 in Supporting Information). This finding manifested that the nanoassembly did not induce apoptotic signaling in the cells, supporting the potential of this nanosensor for cell apoptosis bioimaging.

Live Cell Imaging of Cyt c Release with Aptamer−GO Nanoassembly. To disclose the intracellular localization of

DOI: 10.1021/ja511988w
J. Am. Chem. Soc. 2015, 137, 982−989

the nanosensor, we synthesized a fluorescent nanoassembly by conjugating carboxyfluorescein (FAM) and folate (in 1:1 ratio) to the residual amino groups of PEGylated GO. This FAM modifier was reported to still retain strong fluorescence without being quenched by GO,[13] offering a useful tracker for the localization of this nanosensor. The FAM-modified nanoassembly (15 μg mL^{-1}) was incubated with the cells for 1 h using the serum-free RPMI 1640 culture medium, with subcellular organelles, lysosomes and mitochondria, separately stained using their fluorescent trackers (Lyso@tracker and Mito@tracker, emission peak at 590 nm). We observed that the green channel displayed a bright fluorescence image, which was not colocalized with those (in red pseudo-color) at the orange channel for lysosome and mitochondria trackers (Figure S11 in Supporting Information). This result gave immediate evidence for efficient escape of the nanoassembly from the endosomes or lysosomes with typical cytosolic delivery. This cytosolic, mitochondria-isolated localization of the nanoassembly was also crucial for its selective fluorescence activation response to Cyt c release, because its interaction with Cyt c localized in the intermembrane space of mitochondria was precluded. Moreover, the incorporation of folate modifiers greatly improved the efficiency and selectivity of the nanoassembly to be internalized into cells (FR+) (Figure S12 in Supporting Information). This finding implied that the nanoassembly was uptaken into living cells mainly through a FR-mediated endocytosis pathway,[14] suggesting the potential of this nanosensor for cell-selective imaging. Additionally, we determined the intracellular nanoassembly concentration after incubating 15 μg mL^{-1} nanoassembly with HeLa cells (FR+) for 1 h to be ~150 μg mL^{-1}, evidencing 10-fold concentrating and efficient uptake of the nanoassembly in the cells.

After interrogating *in vitro* response and intracellular delivery characteristics of the nanosensor, we then explored its ability for live cell imaging of Cyt c translocation in apoptotic cells. As anticipated, we only obtained an extremely weak fluorescence signal after incubating HeLa cells (FR+) with the nanoassembly in the serum-free RPMI-1640 medium for 1 h (Figure 3a). This low-background fluorescence was attributed to the spatial isolation of the nanosensor from Cyt c located in the mitochondrial intermembrane space in nonapoptotic cells. It also verified the specificity of the aptamer to the mature heme-containing Cyt c versus apocytochrome c. After the cells were subsequently treated for 1.5 h with different concentrations of staurosporine (STS), a potent apoptosis inducer specifically triggering cytosolic Cyt c release from mitochondria,[15] increasingly brighter red fluorescence images were observed with increasing STS concentrations. In contrast, for HeLa cells (FR+) incubated using the control nanoassembly constructed using nonaptamer DNA and PEGylated GO followed by STS treatment, no bright fluorescence image was obtained. This result further validated the selectivity of the nanosensor in response to Cyt c. Moreover, when STS-induced cells were pretreated with pepstatin A, an inhibitor preventing Cyt c release in cells exposed to STS,[16] we obtained a much weak fluorescence image. A Western blotting assay for plasma extracts in these cells revealed that cytosolic Cyt c concentrations increased with increasing STS concentrations, while decreased after pepstatin A treatment (Figure 3b). This finding was also confirmed by the assays of these plasma extracts using the nanosensor (Figure S13 in Supporting Information). A flow cytometric assay further indicated a substantial fluorescence increase for apoptotic cells when

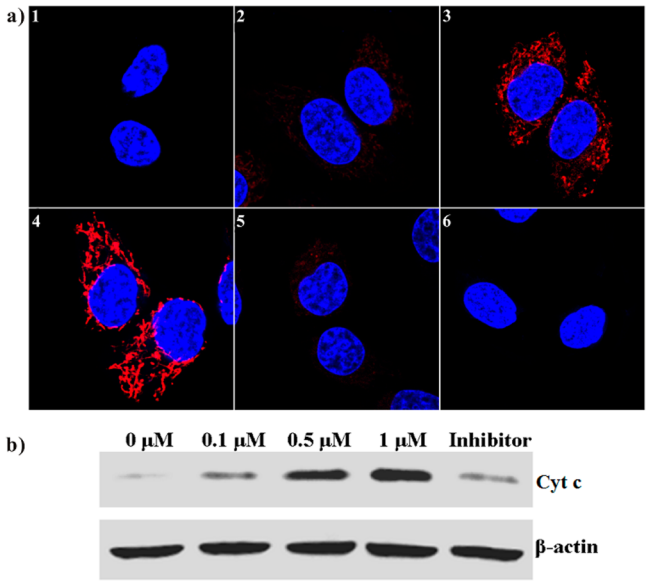

Figure 3. (a) Fluorescence imaging of HeLa cells (FR+) incubated with 15 μg mL^{-1} nanoassembly in serum-free RPMI-1640 medium for 1 h at 37 °C. (1) no treatment, (2) 0.1 μM STS for 1.5 h, (3) 0.5 μM STS for 1.5 h, (4) 1 μM STS for 1.5 h, (5) pretreated with 100 μM pepstatin A for 24 h and incubated with nanoassembly for 1 h followed by 1 μM STS for 1.5 h, (6) incubated with nonaptamer nanoassembly for 1 h followed by 1 μM STS for 1.5 h. (b) Western blotting assay for plasma extracts from corresponding cells. A housekeeping protein β-actin was chosen as the reference.

induced by STS (Figure S14 in Supporting Information). These data revealed a dynamic concentration-dependent fluorescence response to Cyt c, implying the potential of the nanosensor for quantitative imaging of Cyt c release in cell apoptosis.

To verify that the fluorescence activation response was specific to the release of Cyt c from mitochondria into the cytosol during cell apoptosis, the colocalization of Cyt c with mitochondria was interrogated. Because the activated fluorescence signal was derived from the aptamer−Cyt c complex dissociated from GO surface, the localization of Cyt c in the cytosol was able to be visualized using the fluorescence-activated aptamer as the tracker. As shown in Figure 4, when HeLa cells (FR+) were incubated in a nonapoptotic state with the nanoassembly and the mitochondria tracker Mito@tracker, we obtained a very weak fluorescence signal at the red channel for the nanosensor but a bright image at the orange channel (in green pseudo-color) for the mitochondria tracker. The fluorescence image gave a branched filamentous structure, a typical morphology of mitochondria in nonapoptotic cells.[17] On the other hand, after the cells treated using STS, bright fluorescence images were obtained at both channels for the nanoassembly and the Mito@tracker. The green image showed a fragmented bubble-like morphology, indicators of the loss of mitochondria function and the progression of cell apoptosis.[18] Furthermore, the red image appeared as a substantially expanded area of the green image, suggesting a diffusion-like release of Cyt c from mitochondria, which coincided with previous reports on this translocation as simple diffusion through openings in the outer mitochondria membrane.[19] These results gave clear evidence for the cytosolic translocation of Cyt c from mitochondria, testifying the specificity of the nanosensor's fluorescence activation to Cyt c release.

DOI: 10.1021/ja511988w
J. Am. Chem. Soc. 2015, 137, 982−989

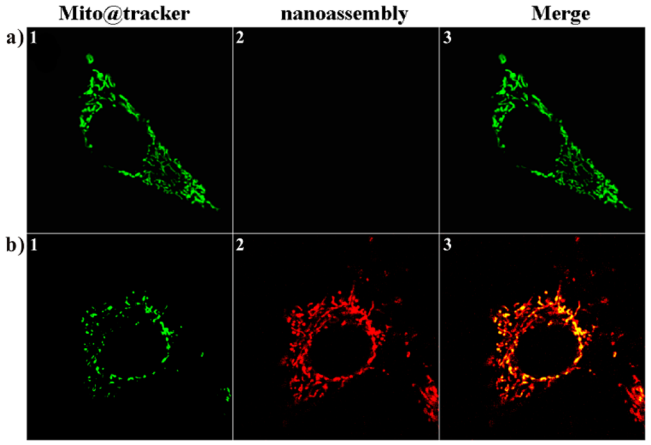

Figure 4. Fluorescence imaging of HeLa cells (FR+). (a) Incubated with 15 μg mL^{-1} nanoassembly for 1 h and mito@tracker for 20 min; (b) incubated with 15 μg mL^{-1} nanoassembly for 1 h, 1 μM STS for 1.5 h and mito@tracker for 20 min.

Imaging of Cyt c Release for Apoptotic Studies. Because of its rapid response (<5 min for the nanoassembly at an estimated intracellular concentration 150 μg mL^{-1}), the nanosensor was able to provide a useful platform for real-time monitoring the release of Cyt c in apoptotic cells. With HeLa cells (FR+) induced by STS, we observed that the fluorescence image gave appreciable brightness after 15 min and reached the maximum intensity after 25 min (Figure 5a and Figure S15a in Supporting Information), indicating that the Cyt c release process was very rapid and completed within ~10 min. This finding verified the previous disclosure that Cyt c release was rapid in many cell types during apoptosis.[7b] This consistency with previous finding also suggested the ability of the nanosensor for real-time visualization of the Cyt c translocation kinetics. Moreover, according to the observation of complete release of Cyt c during cell apoptosis, it revealed that the saturated fluorescence signal obtained in the monitoring was ascribed to the complete release of Cyt c from mitochondria. To shed light on the correlation of Cyt c release to caspase-3 activation, we also performed time-dependent imaging of caspase-3 activation in the STS-induced cells using the commercial intracellular caspase-3 probe (The response time was also <5 min[20]). Interestingly, we observed appreciable caspase-3 activation after 40 min STS treatment, ~25 min later to the appearance of Cyt c translocation (Figure 5b, Figure S15b in Supporting Information). These observations disclosed that cytosolic translocation of Cyt c appeared precedingly with respect to caspase-3 activation during cell apoptosis, which was consistent with the recognized apoptotic signaling in which cytosolic Cyt c was responsible for caspase-9 activation with followed caspase-3 activation.[1,2] In addition, we found that the fluorescence contrast remained increasing for caspase-3 probe through the observation period, indicating a much longer period was required for complete activation of caspase-3. This finding suggested that it took a much longer time for complete activation of caspase-3.[21]

Because of the pivotal role of Cyt c in cell apoptosis, the nanosensor also opened possibilities of directly interrogating critical regulators for apoptotic signaling. To demonstrate the potential, we chose pro- and antiapoptotic members of the B cell lymphoma 2 (BCL-2) protein family, Bax and Bcl-2, and an initiator caspase, caspase-9, for the case study. HeLa cells (FR+) overexpressing Bax or Bcl-2 were obtained by transduction with the recombinant adenovirus containing Bax or Bcl-2 gene (Figure S16 in Supporting Information), while HeLa cells with inhibited caspase-9 activity were obtained by incubation with a potent and selective caspase-9 inhibitor I.[22] These cell lines were incubated with the nanoassembly and the intracellular caspase-3 probe for 1 h followed by treatment with STS (1 μM). It was observed that the cells transduced with the null control adenovirus containing no exogenous genes displayed the same fluorescence activation responses to Cyt c release after STS induction as those obtained with nontransduced HeLa cells (Figure S17 in Supporting Information). This result validated that the transduction of adenovirus had little perturbation to the apoptotic signaling of HeLa cells.

As anticipated, nontransduced HeLa cells, after STS induction for 1 h, gave bright fluorescence signals at the green and the red channels, indicating Cyt c release from mitochondrial and caspase-3 activation in cell apoptosis (Figure 6a). It is important to note that Cyt c formed an aptamer-binding complex in this situation. This observation indeed manifested a new interesting finding that binding of the aptamer did not affect the function of Cyt c in constituting apoptosomes and activating caspases. Surprisingly, we obtained bright fluorescence images throughout the observation period at both the green and the red channels for Bax-overexpressing HeLa cells even without STS treatment (Figure 6b). With reference to the images obtained with nontransduced HeLa cells, this result implied that overexpression of Bax by itself was able to induce the release of Cyt c followed by the activation of caspase-3. The induction of both Cyt c release and caspase-3 activation identified Bax as a pro-apoptotic regulator upstream to Cyt c release. This finding was in good agreement with previous reports that Bax was responsible for mitochondrial outer membrane permeabilization underlying Cyt c release, and

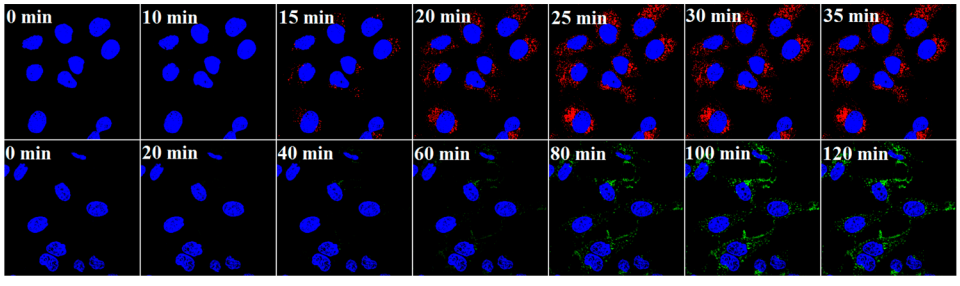

Figure 5. Real-time fluorescence imaging of cell apoptosis in HeLa cells (FR+) incubated with 15 μg mL^{-1} nanoassembly or 9 μM caspase-3 probe for 1 h followed by treatment of 1 μM STS. (a) Time-dependent fluorescence responses for the nanoassembly; (b) time-dependent fluorescence responses for caspase-3 probe.

DOI: 10.1021/ja511988w
J. Am. Chem. Soc. 2015, 137, 982−989

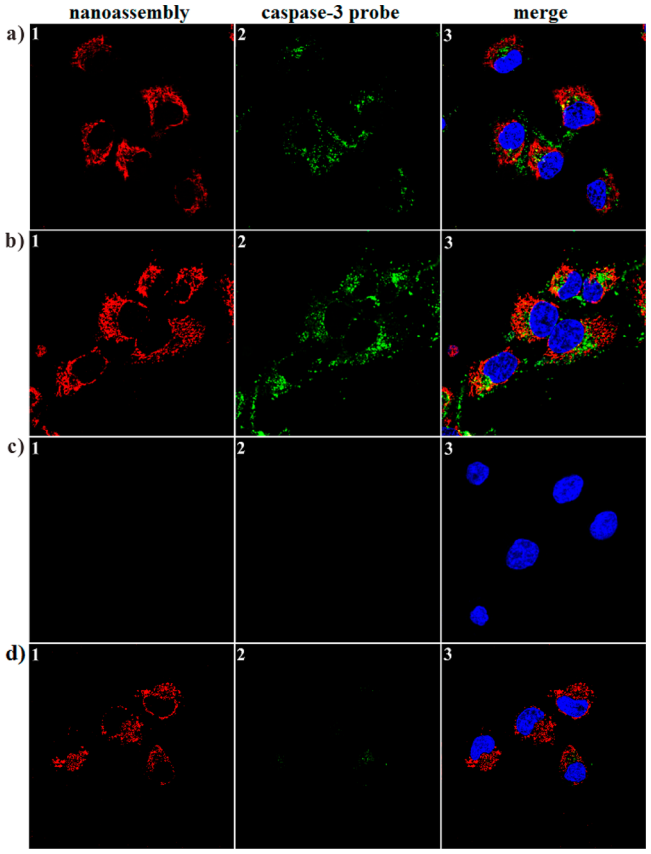

Figure 6. Fluorescence imaging of apoptotic signaling. (a) HeLa cells (FR+) incubating with nanoassembly and caspase-3 probe followed by 1 μM STS for 100 min; (b) Bax overexpressing HeLa cells (FR+) incubating with nanoassembly and caspase-3 probe; (c) Bcl-2 overexpressing HeLa cells (FR+) incubating with nanoassembly and caspase-3 probe followed by 1 μM STS for 100 min; (d) HeLa cells (FR+) incubating with nanoassembly and caspase-3 probe followed by 100 μM caspase-9 inhibitor I for 1 h and then 1 μM STS for 100 min.

Bax overexpression was able to induce cell apoptosis via mitochondrial pathways.[23] On the other hand, no fluorescence activation signals were obtained at both the green and the red channels for the cells overexpressing Bcl-2 even after STS treatment for 1 h (Figure 6c). This observation suggested that Bcl-2 overexpression inhibited the release of Cyt c and the activation of caspase-3. The inhibition of both Cyt c release and caspase-3 activation ascertained Bcl-2 as an anti-apoptotic regulator upstream to Cyt c release. This observation also coincided with the biological function of Bcl-2, which interacted directly with their pro-apoptotic counterparts BAK and BAX and sequestered them in inactive states, thereby preventing mitochondrial outer membrane permeabilization responsible for Cyt c release.[24] Interestingly, the cells incubated with caspase-9 inhibitor I displayed distinct fluorescence responses from the Bax or Bcl-2 overexpressing cells. We obtained a bright fluorescence signal at the red channel while a weakly fluorescent image at the green channel (Figure 6d), indicators of the release of Cyt c without the activation of caspase-3. Because caspase-9 inhibitor I was shown to have no inhibition to caspase-3,[25] this data indicated that in case of inhibited caspase-9 activity, cytosolic release of Cyt c did not result in the activation of caspase-3. This result revealed the essential role of caspase-9 as a molecular player downstream to Cyt c release and upstream to caspase-3 activation, which was consistent with the recognized mechanism of mitochondrial-dependent apoptosis.[1,2]

Besides the possibility of elucidating apoptotic signaling pathway for cell biology, the nanosensor also provided a viable platform for cell-based screening of apoptosis-inducing compounds toward drug development. Five candidate compounds, four known apoptosis inducers, sodium ascorbate, cisplatin, etoposide, and STS, and a cell plasma membrane collapse stimulant digitonin, were examined.[26] HeLa cells (FR +) were incubated with the nanoassembly for 1 h followed by the treatment with individual compound (5 μM in DMSO) for additional 1.5 h. The images obtained revealed that STS gave the highest fluorescence contrast due to Cyt c release, followed sequentially by etoposide, cisplatin and sodium ascorbate, and no fluorescence activation appeared for digitonin (Figure S18 in Supporting Information). This finding implied that STS was the most potent inducer for apoptosis and digitonin did not induce apoptosis despite of its strong destructive activity to plasma membranes. A further inspection by incubating the cells with individual compound of varying concentrations was performed. The data showed that the fluorescence signal remained very weak at increasing concentrations of digitonin but was increasingly intensified at increasing concentrations of STS, etoposide, cisplatin and sodium ascorbate. These results suggested that the nanosensor enabled living cell based quantitative evaluation of apoptosis-inducing efficacy for candidate compounds, thereby providing the possibility for cell-based screening of apoptosis-inducing drugs.

■ CONCLUSION

We developed a novel fluorescence activation nanosensor for imaging of Cyt c that, for the first time, enabled direct visualization of the Cyt c translocation event in apoptotic cells. This was also the first time that spatially selective localization of an activatable sensor had been developed for "turn-on" fluorescence imaging of intracellular translocation events in living cells. The nanosensor was readily synthesized by noncovalent assembly of aptamer DNA on PEGylated GO with folate labels. This construct offered improved detection sensitivity, response rate as well as cellular internalization efficiency for the nanosensor. The nanosensor was shown to exhibit high sensitivity and selectivity, rapid response, large signal-to-background ratio for *in vitro* and intracellular quantification of Cyt c. Real-time monitoring of Cyt c release using this nanosensor gave clear evidence that Cyt c release was rapid, complete, and appeared precedingly with respect to caspase-3 activation during cell apoptosis. It was also found that binding of the aptamer did not affect the function of Cyt c in constituting apoptosomes and activating caspases. Moreover, the nanosensor enabled direct identification of critical regulators upstream or downstream to Cyt c release in the apoptosis pathway and cell-based screening of apoptosis-inducing compounds. In virtue of these advantages and potentials, the developed nanosensor may provide an invaluable platform for apoptotic studies and catalyze the fundamental interrogations of Cyt c-mediated biology.

■ EXPERIMENTAL SECTION

Materials. Cytochrome c (Cyt c), folate, NH_2-PEG-NH_2 with a molecular weight (MW) 1500, carboxyfluorescein-NHS (FAM-NHS), staurosporine (STS), dimethyl sulfoxide (DMSO), sodium ascorbate, cisplatin, etoposide, digitonin, human serum albumin (HSA), insulin, vascular endothelial growth factor (VEGF), platelet-derived growth

DOI: 10.1021/ja511988w
J. Am. Chem. Soc. 2015, 137, 982−989

factor B-chain (PDGF), ferritin, immunoglobulin G (IgG), cysteine, adenosine triphosphate (ATP), isoascorbic acid (AA), *N*-hydroxysuccinimide (NHS), *N*-hydroxysulfosuccinimide sodium salt (Sulfo-NHS) and dicyclohexylcarbodiimide (EDC) were purchased from Sigma-Aldrich (St. Louis, MO). Hoechst 33342, lysosome fluorescent trackers (Lyso@tracker) and mitochondria fluorescent trackers (Mito@tracker) were obtained from Invitrogen (Carlsbad, CA). Graphene oxide (GO) was supplied by Xianfeng Nanomaterials Co. Ltd. (Nanjing, China). Caspase-3 Intracellular Activity Assay Kit and caspase 9 inhibitor I were obtained from Merck Millipore (Darmstadt, Germany). Recombinant adenoviruses containing Bax or Bcl-2 and null control adenoviruses containing no exogenous genes were obtained from Hanbio Biotechnology Co. Ltd. (Shanghai, China). Cytoplasmic and Mitochondrial Protein Extraction Kit was obtained from Sangon Biotech Co. Ltd. (Shanghai, China). Antibodies and reagents for Western blotting (WB) assay were purchased from Mitaka Biotechnology Co. Ltd. (Wuhan, China). HeLa and MCF-7 cell lines were supplied by the cell bank at Xiangya Hospital (Changsha, China). RPMI 1640 cell culture medium was purchased from Thermo Scientific HyClone (Waltham, MA). The DNA aptamer to Cyt c and the nonaptamer DNA were synthesized from Sangon Biotech Co. Ltd. (Shanghai, China), which had the sequences as follows: Aptamer, 5′ Cy5-CCG TGT CTG GGG CCG ACC GGC GCA TTG GGT ACG TTG TTG C-3′;[27] Nonaptamer, 5′ Cy5-ATG ATG CAT CAT CTC TGA AGT AGC GCC GCC GTA TAC TCA C-3′. All other chemicals were of analytical grade and purchased from Sinopharm Chemical Reagent Co. Ltd. (Shanghai, China). All solutions were prepared using ultrapure water, which was obtained through a Millipore Milli-Q water purification system (Billerica, MA), with an electric resistance >18.3 MΩ.

Preparation of Aptamer−Graphene Nanoassembly. The aptamer−graphene nanoassembly was immediately prepared by incubating 1500 μg mL^{-1} PEGylated GO with 5 μM Cy5-tagged DNA aptamer in 10× PB saline (PBS) (1× PBS, pH 7.4, 10 mM KH_2PO_4/K_2HPO_4, 137 mM NaCl, 2.7 mM KCl) for 30 min. The amount of PEGylated GO was optimized by a titration with varying PEGylated GO amount, and the optimal amount was determined according to the value at which the fluorescence decrease became insignificant. The nanoassembly of aptamer and GO was prepared by incubating 500 μg mL^{-1} GO with 5 μM Cy5-tagged DNA aptamer in 10× PBS for 30 min. The amount of GO was optimized by a titration with varying GO amount, and the optimal amount was determined according to the value at which the fluorescence decrease became level off.

Considering the complete fluorescence quenching of DNA aptamer on GO nanosheets, we assumed that 500 nM DNA aptamer was totally assembled on 150 μg mL^{-1} PEGylated GO. Thus, the coverage of DNA aptamer on PEGylated GO nanosheets could be estimated immediately to be ∼3.1 × 10^{11}/cm^2. Likewise, the coverage of DNA aptamer on GO nanosheets was estimated to be ∼8.4 × 10^{11}/cm^2.

Cell Culture and Adenovirus Transduction. HeLa cells and MCF-7 cells were grown in RPMI 1640 medium supplemented with 10% fetal bovine serum, 100 U mL^{-1} penicillin and 100 U mL^{-1} streptomycin at 37 °C in a humidified atmosphere containing 5% CO_2. HeLa cells (FR+, folate receptor expression positive) were obtained from HeLa cells grown in a folate-free cell growth medium for 24 h. HeLa cells (FR-, folate receptor expression negative) were obtained from HeLa cells grown in 5 mM folate-supported cell growth medium for 24 h. The transduction of HeLa cells (FR+) with recombinant adenovirus containing Bax, Bcl-2 or null gene was performed by incubating the cells (1 × 10^5 per well) with the adenovirus (1 × 10^7 per well) for 2 h in a folate-free cell growth medium followed by incubation in fresh folate-free cell growth medium for another 48 h.

***In Vitro* Detection of Cyt c.** The assay of Cyt c was performed by adding 90 μL of the sample of interest in 10 μL of fresh nanoassembly solution containing 1500 μg mL^{-1} PEGylated GO (or 500 μg mL^{-1} GO) and 5 μM Cy5-tagged DNA aptamer in 10× PBS followed by incubation for 30 min at 37 °C. The resulting mixture was immediately subjected to fluorescence measurements. The samples under investigation included Cyt c solutions of varying concentrations in 10× PBS, species coexisting with Cyt c in biological fluids, cytoplasmic protein extract from nonapoptotic HeLa cells, mixtures of 10 μL of Cyt c of different concentrations with 90 μL of cytoplasmic protein extract from nonapoptotic HeLa cells, and cytoplasmic protein extract from apoptotic HeLa cells induced for 1.5 h by STS of different concentrations.

Fluorescence Imaging of Living Cells. Fluorescence imaging of Cyt c translocation in living cells was performed as follows: HeLa cells (FR+) were plated on a 35 mm Petri dish with 10 mm bottom well in the folate-free RPMI 1640 medium for 24 h, then incubated with the nanoassembly solution containing 50 nM aptamer and 15 μg mL^{-1} PEGylated GO in the folate-free RPMI 1640 medium at 37 °C for 1 h for cell uptake of the nanoassembly. After they were washed three times with cold PBS, the cells were incubated with the folate-free fresh RPMI 1640 medium containing STS (or other reagent) of a given concentration for additional 1.5 h at 37 °C. Each well was washed twice with cold PBS before imaging. Fluorescence imaging of the localization for DNA aptamer dissociated from the nanoassembly in living cells was performed using the same protocol except for an additional incubation step after STS induction with 20 nM Mitochondria tracer (Mito@tracker orange) for 20 min before imaging. Fluorescence imaging of caspase-3 activation was performed with HeLa cells (FR+) plated on a 35 mm Petri dish incubated with 9 μM caspase-3 probe in the folate-free RPMI 1640 medium for 1 h. Fluorescence imaging of intracellular localization for the nanoassembly was performed as follows: Cells plated on a 35 mm Petri dish were incubated with the nanoassembly solution containing 50 nM aptamer and 15 μg mL^{-1} PEGylated GO with FAM and folate modifiers in the RPMI 1640 medium (no folate for FR+ cells and 5 mM folate for FR- cells) at 37 °C for 1 h. After they were washed three times with cold PBS, the cells were incubated with the folate-free fresh RPMI 1640 medium containing 20 nM Lysosomes tracer (Lyso@tracker orange) or 20 nM Mitochondria tracer (Mito@tracker orange) for 20 min followed by imaging. The end-point fluorescence images were collected at a sampling speed of 40 μs/pixel with a transmissivity of 20%. The PMT voltage, gain, and offset values were 466, 2, and 20 for blue channel; 587, 2, and 20 for red channel; 407, 2, and 20 for orange channel; and 541, 2, and 20 for green channel, respectively.

Time-dependent fluorescence imaging of Cyt c translocation in living cells was performed as follows: HeLa cells (FR+) plated on a 35 mm Petri dish were incubated with 15 μg mL^{-1} nanoassembly and 9 μM caspase-3 probe in the folate-free RPMI 1640 medium for another 1 h. The cells were then treated with 1 μM STS. The fluorescence imaging was taken immediately after the addition of STS. The real-time fluorescence images were collected at a faster sampling speed of 10 μs/pixel with a transmissivity of 10%. The PMT voltage, gain, and offset values were 756, 2, and 20 for blue channel; 805, 2, and 40 for red channel; and 661, 2, and 19 for green channel, respectively.

■ ASSOCIATED CONTENT

Ⓢ Supporting Information

Experimental details and additional figures. This material is available free of charge via the Internet at http://pubs.acs.org.

■ AUTHOR INFORMATION

Corresponding Author

xiachu@hnu.edu.cn

Notes

The authors declare no competing financial interest.

■ ACKNOWLEDGMENTS

This work was supported by NSFC (21275045, 21190041), NCET-11-0121 and NSF of Hunan (12JJ1004).

■ REFERENCES

(1) Ow, Y. P.; Green, D. R.; Hao, Z.; Mak, T. W. *Nat. Rev. Mol. Cell. Biol.* **2008**, *9*, 532−542.

DOI: 10.1021/ja511988w
J. Am. Chem. Soc. 2015, 137, 982−989

(2) Tait, S. W. G.; Green, D. R. *Nat. Rev. Mol. Cell. Biol.* **2010**, *11*, 621−632.
(3) Shi, Y. *Nat. Struct. Biol.* **2001**, *8*, 394−401.
(4) (a) Degterev, A.; Boyce, M.; Yuan, J. *Oncogene* **2003**, *22*, 8543−8567. (b) Green, D. R.; Kroemer, G. *Science* **2004**, *305*, 626−629.
(5) (a) Jun, Y.; Sheikholeslami, S.; Hostetter, D. R.; Tajon, C.; Craik, C. S.; Alivisatos, A. P. *Proc. Natl. Acad. Sci. U.S.A.* **2009**, *42*, 17735−17740. (b) Wang, H.; Zhang, Q.; Chu, X.; Chen, T.; Ge, J.; Yu, R. *Angew. Chem., Int. Ed.* **2011**, *50*, 7065−7069. (c) Hu, M.; Li, L.; Wu, H.; Su, Y.; Yang, P. Y.; Uttamchandani, M.; Xu, Q. H.; Yao, S. Q. *J. Am. Chem. Soc.* **2011**, *133*, 12009−12020. (d) Shi, H.; Kwok, R. T. K.; Liu, J.; Xing, B.; Tang, B.; Liu, B. *J. Am. Chem. Soc.* **2012**, *134*, 17972−17981. (e) Huang, X.; Swierczewska, M.; Choi, K. Y.; Zhu, L.; Bhirde, A.; Park, J.; Kim, K.; Xie, J.; Niu, G.; Lee, S.; Chen, X. *Angew. Chem., Int. Ed.* **2012**, *51*, 1625−1630.
(6) (a) Uren, R. T.; Dewson, G.; Bonzon, C.; Lithgow, T.; Newmeyer, D. D.; Kluck, R. M. *J. Biol. Chem.* **2005**, *280*, 2266−2274. (b) Trusova, V. A.; Gorbenko, G. P.; Molotkovsky, J. G.; Kinnunen, P. K. *Biol. J.* **2010**, *99*, 1754−1763.
(7) (a) Waterhouse, N. J.; Trapani, J. A. *Cell Death Differ.* **2003**, *10*, 853−855. (b) Goldstein, J. C.; Munoz-Pinedo, C.; Ricci, J.; Adams, S. R.; Kelwkar, A.; Schuler, M.; Tsien, R. Y.; Green, D. R. *Cell Death Differ.* **2005**, *12*, 453−462.
(8) (a) Huang, Y. C.; Ge, B.; Sen, D.; Yu, H. *J. Am. Chem. Soc.* **2008**, *130*, 8023−8029. (b) Lau, P. S.; Coombes, B. K.; Li, Y. *Angew. Chem., Int. Ed.* **2010**, *49*, 7938−7942. (c) Keefe, A. D.; Pai, S.; Ellington, A. *Nat. Rev. Drug Discovery* **2010**, *9*, 537−550. (d) Zhang, H.; Li, F.; Dever, B.; Li, X. F.; Le, X. C. *Chem. Rev.* **2013**, *113*, 2812−2841. (e) Tan, W.; Donovan, M. J.; Jiang, J. *Chem. Rev.* **2013**, *113*, 2842−2862. (f) Xing, H.; Hwang, K.; Li, J.; Torabi, S.; Lu, Y. *Curr. Opin. Chem. Eng.* **2014**, *4*, 79−87. (g) Dokukin, V.; Sliverman, S. K. *Chem. Commun.* **2014**, *50*, 9317−9320.
(9) (a) Lu, C.; Yang, H.; Zhu, C.; Chen, X.; Chen, G. *Angew. Chem., Int. Ed.* **2009**, *48*, 4785−4787. (b) Wang, Y.; Li, Z.; Hu, D.; Lin, C.; Li, J.; Lin, Y. *J. Am. Chem. Soc.* **2010**, *132*, 9274−9276. (c) Tan, X.; Chen, T.; Xiong, X.; Mao, Y.; Zhu, G.; Yasun, E.; Li, C.; Zhu, Z.; Tan, W. *Anal. Chem.* **2012**, *84*, 8622−8627.
(10) Chen, C.; Ke, J.; Zhou, X. E.; Yi, W.; Brunzelle, J. S.; Li, J.; Yong, E.; Xu, H. E.; Melcher, K. *Nature* **2013**, *500*, 486−490.
(11) He, S.; Song, B.; Li, D.; Zhu, C.; Qi, W.; Wen, Y.; Wang, L.; Song, S.; Fang, H.; Fan, C. *Adv. Funct. Mater.* **2010**, *20*, 453−459.
(12) (a) Bhuyan, A.; Varshney, A.; Mathew, M. *Cell Death Differ.* **2001**, *8*, 63−69. (b) Waterhouse, N.; Goldstein, J. C.; Ahsen, O. V.; Schuler, M. S.; Newmeyer, D. D.; Green, D. R. *J. Cell. Biol.* **2001**, *153*, 319−328.
(13) Peng, C.; Hu, W.; Zhou, Y.; Fan, C.; Huang, Q. *Small* **2010**, *6*, 1686−1692.
(14) Feng, D.; Song, Y.; Shi, W.; Li, X.; Ma, H. *Anal. Chem.* **2013**, *85*, 6530−6535.
(15) (a) Sawa, A.; Widgand, G. W.; Cooper, J.; Margolis, R. L.; Sharp, A. H.; Lawler, J. F.; Greenamyre, J. T.; Snyder, S. H.; Ross, C. A. *Nat. Med.* **1999**, *5*, 1194−4498. (b) Scarlett, J. L.; Sheard, P. W.; Hughes, G.; Ledgerwood, E. C.; Ku, H.; Murphy, M. P. *FEBS. Lett.* **2000**, *475*, 267−272. (c) Chua, B. T.; Volbracht, C.; Tan, K. O.; Li, R.; Yu, V. C.; Li, P. *Nat. Cell Biol.* **2003**, *5*, 1083−1089.
(16) Johansson, A.; Steen, H.; Ollinger, K.; Roberg, K. *Cell Death Differ.* **2003**, *10*, 1253−1259.
(17) (a) Karbowski, M.; Youle, R. J. *Cell Death Differ.* **2003**, *10*, 870−880. (b) Krumova, K.; Greene, L. E.; Cosa, G. *J. Am. Chem. Soc.* **2013**, *135*, 17135−17143.
(18) (a) Scarlett, J. L.; Sheard, P. W.; Hughes, G.; Ledgerwood, E. C.; Ku, H.; Murphy, M. P. *FEBS. Lett.* **2000**, *475*, 267−272. (b) Gao, W.; Pu, Y.; Luo, K. Q.; Chang, D. C. *J. Cell. Sci.* **2001**, *114*, 2855−2862.
(19) (a) Petronilli, V.; Penzo, D.; Scorrano, L.; Bernardi, P.; Lisa, F. D. *J. Biol. Chem.* **2001**, *276*, 12030−12034. (b) Fiskum, G.; Starkov, A.; Polster, B. M.; Chinopoulos, C. *Ann. N.Y. Acad. Sci.* **2003**, *991*, 111−119.
(20) Packard, B. Z.; Toptygin, D. D.; Komoriya, A.; Brand, L. *Method. Enzymol.* **1997**, *278*, 15−23.
(21) (a) Wood, D. E.; Newcomb, E. W. *J. Biol. Chem.* **1999**, *274*, 8309−8315. (b) Hu, B. R.; Liu, C.; Ouyang, Y.; Blomgren, K.; Siesjo, B. K. *J. Cerebr. Blood Flow Metab.* **2000**, *20*, 1294−1300.
(22) (a) Li, P.; Nijhawan, D.; Budihardjo, I.; Srinivasula, S. M.; Ahmad, M.; Alnemri, E. S.; Wang, X. *Cell* **1997**, *91*, 479−489. (b) Ozoren, N.; Kim, K.; Burns, T. F.; Dicker, B. D.; Moscioni, A. D.; El-Deiry, W. S. *Cancer. Res.* **2000**, *60*, 6259−6265. (c) Thomas, W. D.; Zhang, X.; Franco, A.; Nguyen, T.; Hersey, P. *J. Immunol.* **2000**, *165*, 5612−5620. (d) Strigrtwald, K.; Behbehani, G. K.; Combs, K. A.; Barton, M. C.; Groder, J. *Mol. Cancer. Res.* **2005**, *3*, 78−89.
(23) (a) Jurgensmeier, J. M.; Xie, Z.; Deveraux, Q.; Ellerby, L.; Bredesen, D.; Reed, J. *Proc. Natl. Acad. Sci. U.S.A.* **1998**, *95*, 4997−5002. (b) Eskes, R.; Antonsson, B.; Osen-Sand, A.; Montessuit, S.; Richter, C.; Sadoul, R.; Mazzei, G.; Nichols, A.; Martinou, J. *J. Cell. Biol.* **1998**, *143*, 217−224. (c) Smaili, S.; Hsu, Y.; Sanders, K.; Russell, J.; Youle, R. *Cell Death Differ.* **2001**, *8*, 909−920.
(24) (a) Yang, J.; Liu, X.; Bhalla, K.; Kim, C. N.; Ibrado, A. M.; Cai, J.; Peng, T.; Jones, D. P.; Wang, X. *Science* **1997**, *275*, 1129−1132. (b) Kluck, R. M.; Bossy-Wdtzel, E.; Green, D. R.; Newmeyer, D. D. *Science* **1997**, *275*, 1132−1136.
(25) (a) Ozoren, N.; Kim, K.; Burns, T. F.; Dicker, B. D.; Moscioni, A. D.; El-Deiry, W. S. *Cancer Res.* **2000**, *60*, 6259−6265. (b) Strigrtwald, K.; Behbehani, G. K.; Combs, K. A.; Barton, M. C.; Groder. *J. Mol. Cancer Res.* **2005**, *3*, 78−89.
(26) (a) Kang, J. S.; Cho, D.; Kim, Y. I.; Hahm, E.; Kim, Y. S.; Jin, S. N.; Kim, H. N.; Kim, D.; Hur, D.; Par, H.; Wang, Y. I.; Lee, W. J. *J. Cell. Physiol.* **2005**, *204*, 192−197. (b) Herrmann, R.; Fayad, W.; Schwarz, S.; Berndtsson, M.; Linder, S. *J. Biomol. Screening* **2008**, *13*, 1−8.
(27) Lau, L. P. M.; Ngan, E. K. S.; Loo, J. F. C.; Suen, Y. K.; Ho, H. P.; Kong, S. K. *Biochem. Biophys. Res. Commun.* **2010**, *395*, 560−564.

DOI: 10.1021/ja511988w
J. Am. Chem. Soc. 2015, 137, 982−989